BULLETIN DE L'ASSOCIATION MINERALOGIQUE DU CANADA

THE CANADIAN MINERALOGIST

JOURNAL OF THE MINERALOGICAL ASSOCIATION OF CANADA

Volume 35 August 1997 Part 4

The Canadian Mineralogist
Vol. 35, pp. 805-815 (1997)

"INVISIBLE" GOLD IN SULFIDES FROM THE CAMPBELL MINE, RED LAKE GREENSTONE BELT, ONTARIO: EVIDENCE FOR MINERALIZATION DURING THE PEAK OF METAMORPHISM

CHARLES A. TARNOCAI[1] AND KÉIKO HATTORI[1]

Department of Geology, University of Ottawa, Ottawa, Ontario K1N 6N5

LOUIS J. CABRI[1]

CANMET, 555 Booth Street, Ottawa, Ontario K1A 0G1

ABSTRACT

The Au content of pyrite and arsenopyrite from the Campbell mine, Red Lake mining camp, Ontario, has been established by secondary-ion mass spectrometry (SIMS). All Au contents significantly exceed the minimum detection-limits of the technique (36 ppb in arsenopyrite, 193 ppb in pyrite). Arsenopyrite is characterized by high contents of "invisible" Au (up to 0.56 wt%). Coarse-grained arsenopyrite displays Au zoning, and fine-grained arsenopyrite generally displays a uniform Au content. Gold is present in low concentrations in pyrite (up to 168 ppm), and elevated Au is related to As-rich zones. The host rocks at the mine have experienced low-pressure amphibolite-grade metamorphism. We consider it unlikely that compositional zoning could survive metamorphic recrystallization. Textural relations between gahnite and auriferous arsenopyrite, and the presence of auriferous arsenopyrite inclusions in garnet, indicate that the introduction of Au was synchronous with peak conditions of metamorphism.

Keywords: arsenopyrite, pyrite, metamorphism, "invisible" gold, secondary-ion mass spectrometry (SIMS), crystal chemistry, Archean gold mineralization, Campbell mine, Red Lake, Ontario.

SOMMAIRE

La teneur en or de la pyrite et de l'arsénopyrite de la mine Campbell, du camp minier de Red Lake, en Ontario, a été déterminée par spectrométrie de masse des ions secondaires (SIMS). Toutes les teneurs en Au dépassent largement le seuil de détection de la méthode (36 ppb dans l'arsénopyrite, 193 ppb dans la pyrite). L'arsénopyrite possède des teneurs élevées en or "invisible" (jusqu'à 0.56% en poids). L'arsénopyrite à grains grossiers fait preuve de zonation dans la distribution de l'or, tandis que l'arsénopyrite à grains fins possède en général une teneur uniforme. De plus faibles concentrations d'or sont présentes dans la pyrite (jusqu'à 168 ppm), et les teneurs les plus élevées coïncident avec les zones riches en As. Les roches-hôtes du gisement ont subi un métamorphisme dans le faciès amphibolite à faible pression. Nous n'entrevoyons pas la possibilité que la zonation dans ces minéraux puisse survivre la recristallisation métamorphique. Les relations texturales impliquant la gahnite et l'arsénopyrite aurifère, aussi bien que la présence d'inclusions d'arsénopyrite aurifère dans le grenat, indiquent que l'introduction de l'or a eu lieu lors du paroxysme métamorphique.

(Traduit par la Rédaction)

[1] *E-mail addresses*: ctarnoc@science.uottawa.ca, khattori@uottawa.ca, louis.cabri@cc2smtp.nrcan.gc.ca

Mots-clés: arsénopyrite, pyrite, métamorphisme, or "invisible", spectrométrie de masse des ions secondaires, chimie cristalline, minéralisation aurifère archéenne, mine Campbell, Red Lake, Ontario.

INTRODUCTION

The Campbell mine, at Red Lake, northwestern Ontario, exploits an Archean lode-Au deposit; past production and present reserves amount to approximately 344 tonnes of Au. The deposit is hosted within mafic-ultramafic volcanic rocks; it is situated at the transition between the upper greenschist and lower amphibolite facies (Andrews *et al.* 1986, Tarnocai & Hattori 1994). The host rocks have been metamorphosed at temperatures ranging between 450 and 500°C, and approximately 2–3 kilobars pressure (Tarnocai & Hattori 1996). Wallrocks in the upper and western portions of the deposit contain upper-greenschist-facies mineral assemblages, whereas those in the deeper and eastern portions of the deposit contain lower-amphibolite-facies assemblages. The upper-greenschist-facies alteration assemblages include chlorite and white mica (muscovite and paragonite); the lower-amphibolite-facies alteration assemblages include magnesian tschermakite, gedrite, almandine, and cordierite. The peak metamorphic assemblage does not exhibit significant retrogression, indicating that the post-peak hydrothermal activity was minor. Ore veins in amphibolite-facies domains may contain hornblende and gahnite ($ZnAl_2O_4$). Arsenopyrite occurs in veins and wallrocks, and displays a strong spatial association with ore at the Campbell mine.

Very high Au grades occur in quartz–arsenopyrite ore samples that contain few visible Au grains. Spectacular leaf gold occurs in fractures that cut quartz–arsenopyrite ore. This relationship suggests that ores contain significant refractory Au, and that the Au may be remobilized locally into late fractures.

Gold mineralization in greenschist-facies terranes is considered to postdate peak metamorphism (Robert & Brown 1981, Wong *et al.* 1991), but the timing of Au mineralization in amphibolite-facies terranes is under debate. Pre-metamorphic Au mineralization has been reported at the Big Bell deposit, Yilgarn Block, Australia (Phillips & de Nooy 1988). Syn-peak metamorphic Au deposits have been documented in the Southern Cross Province of the Yilgarn Block, and at Main Hill and Breccia Hill in the Pilbara Block (Bloem *et al.* 1994, Neumayr *et al.* 1993), and at Musselwhite in the Superior Province (Hall & Riggs 1986). Syn- to post-peak metamorphic Au mineralization has been suggested for the Con mine in the Slave Province (McDonald *et al.* 1993), and post-peak metamorphic introduction of Au is indicated at the Detour mine (Marmont 1986), in the Superior Province.

Results from scanning electron microscopy (SEM) and secondary-ion mass spectrometry (SIMS) analysis of pyrite and arsenopyrite from the Campbell mine are presented in this paper. The occurrence of zoned auriferous arsenopyrite, and the textural relations between auriferous arsenopyrite and both garnet and gahnite, are used to constrain the timing of introduction of Au relative to metamorphism.

SAMPLE SELECTION

Ores at the Campbell mine are hosted by foliation-parallel, northwest-trending quartz–carbonate veins, and by foliation-oblique conjugate shears (Zhang *et al.*, in press), quartz–carbonate veins and pipe-like quartz–arsenopyrite replacement bodies. Both styles of mineralization have caused an envelope of wallrock alteration that contains disseminated arsenopyrite. Typical samples of ore were selected for SIMS and SEM analyses, from both foliation-parallel (1925 stope, F2 zone; and 2451–5 stope,

TABLE 1. SAMPLE LOCATIONS AND DESCRIPTIONS, ORE ZONES IN THE CAMPBELL MINE, RED LAKE BELT, ONTARIO

Ore Zone	Stope	Ore type	Mineralogy
F2	1925	Foliation-parallel quartz-ankerite vein.	Predominantly quartz, ankerite, pyrrhotite; minor pyrite, scheelite, and tourmaline. 2-3 vol. % euhedral arsenopyrite.
P	2451-6 (EW)	Foliation-oblique, E/W-trending quartz veins.	Quartz, ankerite, pyrrhotite, pyrite, 3 vol. % fine-grained euhedral arsenopyrite.
P	2451-6 (NS)	Foliation oblique N/S trending quartz-arsenopyrite replacement zone.	Quartz with 10 vol. % euhedral arsenopyrite. Minor pyrrhotite and trace magnetite.
P	2451-5	Foliation-parallel quartz-ankerite vein.	Predominantly quartz, ankerite, 5 vol. % euhedral arsenopyrite, 3-5 vol. % patchy pyrrhotite aggregates, minor pyrite, trace sphalerite and stibnite.
L	1854	Foliation-oblique quartz-pyrite-arsenopyrite replacement zone.	Quartz, ankerite, 8 vol. % patchy pyrite, 3 vol. % fine-grained arsenopyrite, minor chromian muscovite, trace pyrrhotite and tourmaline.

P zone) and foliation-oblique (2451–6 stope N/S and EW structures, P zone; and 1854 stope, L zone) ore structures. The host rocks for these samples have been subjected to upper-greenschist- (P and F2 zone) to lower-amphibolite-facies (L zone) metamorphism. Sample locations and descriptions are provided in Table 1. Quantitative SIMS analysis was conducted on euhedral to subhedral grains of arsenopyrite, 40 to 150 μm in size, and on subhedral grains of pyrite 30 to 800 μm in size. Arsenopyrite used for the SEM study was also obtained from a quartz–arsenopyrite replacement zone in the 1756–2E stope, NL zone, which contains 5–10 vol.% gahnite, biotite, and ankerite, and from wallrocks in the 2451–5 P zone.

Analytical Procedures

Rock samples were crushed and hand-sorted to produce pyrite and arsenopyrite separates. Mineral separates were mounted in a mixture of epoxy and 10 wt% graphite, and polished. Sulfide grains were checked for inclusions by reflected light microscopy, and with a JEOL JSM–6400 scanning electron microscope at up to 43,000× magnification. Gold inclusions 100–200 nm across would be recognizable at this magnification by SEM.

TABLE 2. SUMMARY OF THE SIMS EXPERIMENTAL PARAMETERS

Primary-Ion Beam and Polarity	Cs^+
Secondary-Ion Polarity	Negative
Matrix Masses Measured	$^{57}Fe_2{+}^{32}S$
Primary-Beam Current	300-350 nA
Primary-Beam Accelerating Voltage	10 kV
Impact Energy	14.5 kV
Field-Aperture Diameter	750 μm
Contrast-Diaphragm Diameter	400 μm
Raster	250 μm
Image Field	150 μm
Diameter of Analysis Area	62.5 μm
Acquisition rate	1 s $cycle^{-1}$
Implanted standards	arsenopyrite, pyrite
Implantation fluence, species	$2.5x10^{13}$ ions $^{197}Au/cm^2$
Mass resolution	~2,000 m/Δm
Energy offset	none
Minimum detection limits: arsenopyrite	avg. 36 (28- 50) ppb Au
pyrite	avg. 193 (119-266) ppb Au
Graphite-loaded polished section	carbon-coated
Depth of analyzed profiles	0.3 - 2.0 μm

The scanning electron microscope, with an attached Link EXL energy-dispersion spectrometer (EDS), was used to quantitatively determine major-element compositions of sulfides, and to qualitatively investigate the location of Au in zoned crystals of arsenopyrite. Major-element determinations were carried out for 150 s at an accelerating voltage of 20 kV, and a beam current of 0.8 nA, using pyrite for Fe and S, NiAs for As, and $CoAs_2$ as standards. Accuracy is ±1% of the reported values for these elements. Because the minimum excitation-potential for elements with high mass-numbers is relatively large, and the $K\alpha$ line for Au (2.12 keV) is obscured by the $K\alpha$ line for sulfur (2.308 keV), the accelerating voltage was increased to 25 keV to qualitatively examine the Au$L\alpha_1$ peak at 9.711 keV in zoned arsenopyrite.

A Cameca IMS-4f double-focusing, magnetic-sector secondary-ion mass spectrometer was used to determine the Au contents of the sulfide samples. The operating conditions of the spectrometer are listed in Table 2. The collector was set at high mass-resolution (m/Δm ≈ 2000) to alleviate molecular mass-interferences associated with ^{197}Au. Local calibrations of the magnet were made as described by Cabri & McMahon (1995), followed by depth profiles on implanted standards (*e.g.*, Chryssoulis *et al.* 1989). The ^{197}Au mass and one or two other masses (*e.g.*, ^{56}Fe, $^{57}Fe_2 + {}^{32}S$) were recorded, in order to monitor the system stability, the integrity of the sample, and to provide a reference mass for RSF (relative-sensitivity factor) calculations. Integrated counts for matrix mass $^{57}Fe_2 + {}^{32}S$ subsequently were used for the RSF calculations at the conclusion of the depth profile. The RSF is a multiplying factor used to convert the experimentally measured ion-count rate to atom density, and is unique to the sample matrix (pyrite and arsenopyrite in this study), the operating conditions, and the mass of calibrating matrix. Following depth-profiling of the implanted standard, the crater depths were measured across their lengths and widths using a Tencor Alpha-Step 200 profilometer. The RSF values were then determined using SIMS Instrument Control System software, version 4.0, obtained from Charles Evans and Associates (Cabri & McMahon 1995). Minimum detection-limits determined during calibration are provided in Table 2. Depth profiles were then acquired on each mineral selected for analysis, using the same analytical procedures as for the implanted standards. Counts for ^{197}Au and the reference matrix-mass from the mineral samples were obtained by depth-profiling, and the Au concentration calculated using the procedure described by Larocque *et al.* (1995a).

Direct-ion images of selected elemental- and molecular-ion species were acquired by operating the instrument in the ion-microscope mode (which is similar to optical microscopy in principle), while retaining high mass-resolution using a primary-ion beam of large diameter to illuminate the sample surface. Secondary ions are emitted from all points illuminated by the beam in a planar electrostatic field, and the lateral distribution of secondary ions is retained through the double-focusing mass spectrometer system. Following energy and mass filtering, the resulting image is recorded on a resistive anode encoder. The encoder is a pulse-counting, position-computing device capable of localizing ion signals in the image plane of the detector, as well as recording the ion intensity in the image. For the present study, acquisition times ranged from 30 to 60 s, depending

TABLE 3. Au CONTENT OF ARSENOPYRITE, AS DETERMINED BY SIMS

Grain No.	Ore Zone	Location*	Au (ppm)#
1	F2	1925	122
2	F2	1925	2942
3	F2	1925	1262
4	F2	1925	103
5	F2	1925	1557
6	F2	1925	1992
7	F2	1925	2716
8	F2	1925	5610
9	F2	1925	1115
10	F2	1925	1326
11	F2	1925	540
12	P	2451-6(EW)	1607
13	P	2451-6(EW)	4522
14	P	2451-6(EW)	1844
15	P	2451-6(EW)	620
16	P	2451-6(EW)	208
17	P	2451-6(EW)	118
18	P	2451-6(EW)	2896
19	P	2451-6(NS)	1955

* Stope location.
\# ppm by weight

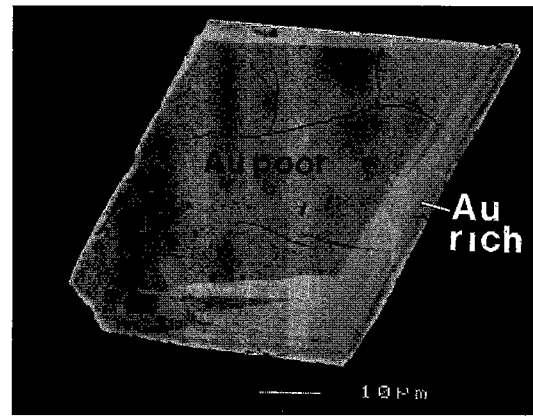

FIG. 1. Back-scattered electron image of arsenopyrite. Light grey margin is Au- and As-rich, and S-poor compared to the darker core. Gold inclusions were not observed by SEM at 43,000× magnification. Note the sharp boundary between the core and rim. Image taken at an accelerating voltage of 25 kV, and a beam current of 3.06 nA.

on the concentration and sensitivity of the selected species. Minimum detection-limits for Au in arsenopyrite were 36 ppb and 193 ppb for pyrite. Analysis of the standard gives an accuracy of 10–15% of the reported value.

RESULTS

Pyrite and arsenopyrite from ore in the Campbell mine contain elevated concentrations of Au. Arsenopyrite has up to 0.56 wt% Au (Table 3), and pyrite has up to 168 ppm Au (Table 4). All grains contain Au at concentrations well above the minimum detection-limit established by SIMS. Grain 8, having 0.56 wt% Au, also shows a Au$L\alpha_1$ peak by SEM–EDS. Grain 7, containing 2,715 ppm Au, lacks a clear Au$L\alpha_1$ peak, indicating that greater than 2,700 ppm Au is required for detection of Au by SEM–EDS.

When viewed with back-scattered-electron imaging (BSE), coarse-grained crystals (>50 µm) of arsenopyrite display compositional zoning (Fig. 1). Zoning generally is more complex in arsenopyrite from the ore veins, as compared to wallrock arsenopyrite. The boundary between core and rim is sharp and irregular. Rims are bright compared to cores, indicating that the average atomic mass of the rims is greater than that of the cores. The rim from grain 8 (Fig. 2) shows a Au$L\alpha_1$ peak, which is absent in the core, and shows that the rims are relatively rich in Au. SIMS ^{197}Au imaging indicates that the rim of zoned grains of arsenopyrite is enriched in Au (Fig. 2), which is compatible with BSE images and the presence of the Au$L\alpha_1$ peak. SIMS imaging also shows that small grains of arsenopyrite are uniformly enriched in Au (Fig. 2).

On the basis of similarities in electron reflectance between Au-rich rims of coarse-grained arsenopyrite and adjacent small grains of unzoned Au-rich arsenopyrite, we suggest that the deposition of fine-grained Au-rich arsenopyrite was synchronous with the growth of an Au-rich rim on the coarse grains. The composition of arsenopyrite (Table 5) indicates that the Au-rich rims are S-poor and As-rich compared to the Au-poor cores. The sum of As and S is relatively constant at ~66 atom % in all arsenopyrite grains. The arsenopyrite formula is calculated on the basis of one atom, and site allocations were based on the data of Wood & Strens (1979). Antimony is included in the *XY* site, on the basis of the similarity of its geochemical properties to those of As. Sums of *M* cations and *XY* site ions are nearly ideal at ~33.3 and ~66.6 atom %, respectively.

Pyrite displays complex Au zoning, which is moderately correlated to elevated As (Fig. 3). Gold contents in pyrite are much lower than those in arsenopyrite (Table 4).

Gahnite occurs in quartz–arsenopyrite ores in the eastern and deeper portions of the Campbell mine. Gahnite is euhedral to subhedral, occurring as individual crystals

TABLE 4. Au CONTENT OF PYRITE, AS DETERMINED BY SIMS

Grain No.	Ore Zone	Location*	Au (ppm)#
1	P	2451-5	8.5
2	P	2451-5	1.5
3	P	2451-5	0.6
4	F2	1925	0.1
5	F2	1925	0.3
6	F2	1925	0.2
7	F2	1925	0.1
8	L	1854	9.8
9	L	1854	2.6
10	L	1854	136
11	L	1854	168
12	P	2451-6(EW)	0.2
13	P	2451-6(EW)	0.5

* Stope location.
\# ppm by weight

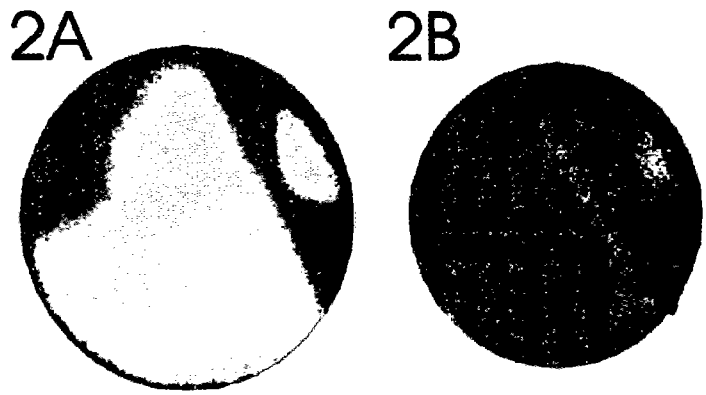

FIG. 2. SIMS direct-ion images of Au and S in arsenopyrite grains. The image of ^{34}S (Fig. 2A) outlines the arsenopyrite grains; the image in Figure 2B shows the distribution of ^{197}Au in arsenopyrite. Colored areas are relatively S and Au-rich, respectively. The large crystal of arsenopyrite in the center of the image (grain 8, Table 2) displays a Au-rich rim. The small crystal in the upper right is uniformly Au-rich. Sample from the P zone, 2451 stope. Acquisition times were 30 s for ^{34}S, 60 s for ^{197}Au. Fields of view are all 62.5 μm.

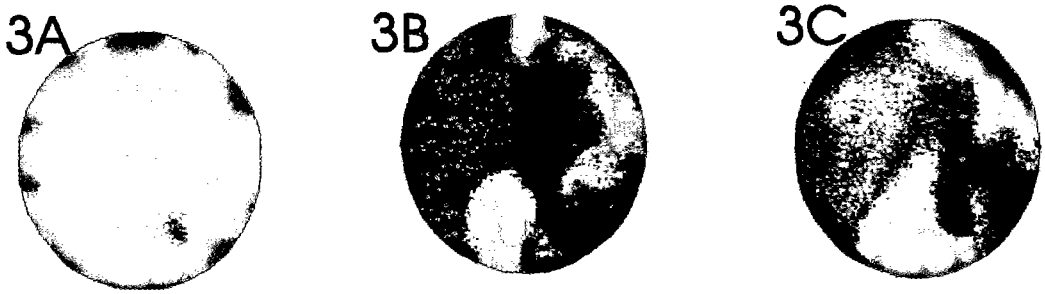

FIG. 3. SIMS direct-ion images of Au, S, and As in pyrite grains. Image 3A shows $^{57}Fe_2 + ^{32}S$, and outlines a pyrite grain that fills the field of view. Images 3B and 3C show the distribution of ^{197}Au and ^{75}As within pyrite, respectively. Yellow and red areas in the ^{197}Au and ^{75}As images are relatively Au- and As-rich, respectively. Note that the patchy zonations of Au enrichment are moderately well correlated with ^{75}As-rich areas. Sample from the L zone, 1854 stope. Acquisition times were 30 s for $^{57}Fe_2 + ^{32}S$, 45 s for ^{197}Au, 45 s for ^{75}As. Fields of view are all 62.5 μm.

TABLE 5. COMPOSITION OF ARSENOPYRITE, AS DETERMINED BY SEM–EDS

	#8, rim	#8, core	#7, rim	#7, core
Fe	36.22	36.71	35.22	36.32
Zn	0.00	0.00	0.22	0.00
Cu	0.00	0.17	0.00	0.00
Sb	0.90	0.85	0.00	1.10
As	41.10	41.37	46.27	41.67
S	22.47	23.61	20.38	22.90
Total	100.69	102.71	102.09	101.99
Formula (basis 1 atom per formula unit)				
Fe	0.340	0.336	0.334	0.337
Zn	0.000	0.000	0.002	0.000
Cu	0.000	0.001	0.000	0.000
ΣM site	0.340	0.337	0.336	0.337
Sb	0.004	0.004	0.000	0.005
As	0.288	0.282	0.327	0.288
S	0.368	0.377	0.337	0.370
ΣXY site	0.660	0.663	0.664	0.663
Total	1.000	1.000	1.000	1.000
As+S	0.656	0.659	0.664	0.658
As+Fe	0.628	0.618	0.661	0.625
As/Fe	0.847	0.839	0.979	0.855
As/S	0.793	0.748	0.970	0.778

Cobalt and nickel were below detection limits. Gold not reported because of insufficient counts at 20 kV accelerating voltage. Refer to analytical procedure.

or as banded aggregates. Rosettes of euhedral arsenopyrite mantle gahnite, and fine-grained euhedral to subhedral arsenopyrite forms inclusions in bands of gahnite (Fig. 4). Arsenopyrite from gahnite-bearing ore displays complex zoning, with a dark core and a bright, banded rim. A dark growth-band is present locally along the margin of zoned grains (Fig. 5).

Almandine occurs in altered wallrocks from the eastern portions of the deposit. Garnet growth was clearly syntectonic, as evidenced by helicoidal trails of inclusions (Fig. 6) of quartz, pyrrhotite, magnetite, and arsenopyrite. Arsenopyrite inclusions within almandine display a bright rim and a dark core in BSE images (Fig. 7). Their zoning is identical to the zoning in arsenopyrite grains outside of garnet. Arsenopyrite from the wallrocks and veins have a core that occasionally displays fractures, which are filled with arsenopyrite that is similar in brightness to that in the rim in BSE images (Fig. 7).

Discussion

Invisible gold in sulfides

Invisible Au is defined as Au that occurs as a structurally bound component in a sulfide mineral, or as "colloidal" Au inclusions less than 0.1 μm in size (Boyle 1979). The presence of Au as a structural

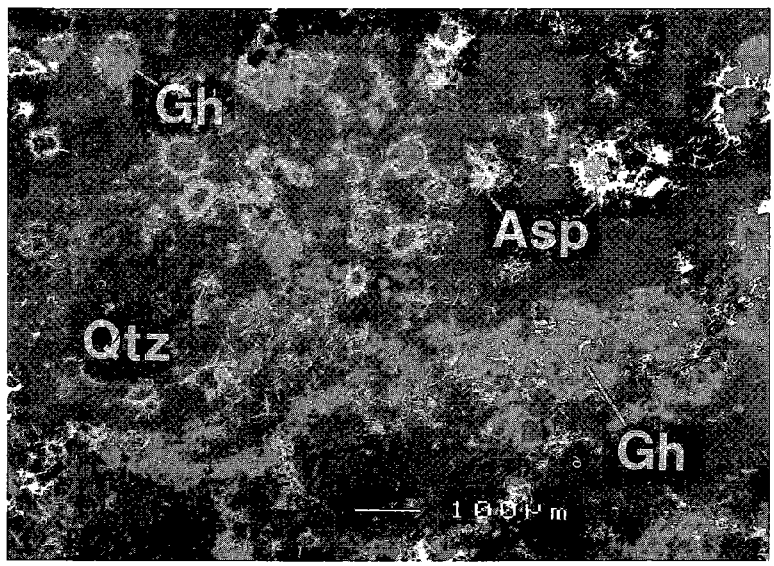

FIG. 4. Back-scattered electron image of arsenopyrite and gahnite. Arsenopyrite (Asp) occurs as rosettes that envelop gahnite (Gh), and also form inclusions within gahnite crystals. Euhedral prisms of arsenopyrite also occur within bands of gahnite in a quartz (Qtz) matrix. Quartz–arsenopyrite replacement ore from the 17th level, L zone.

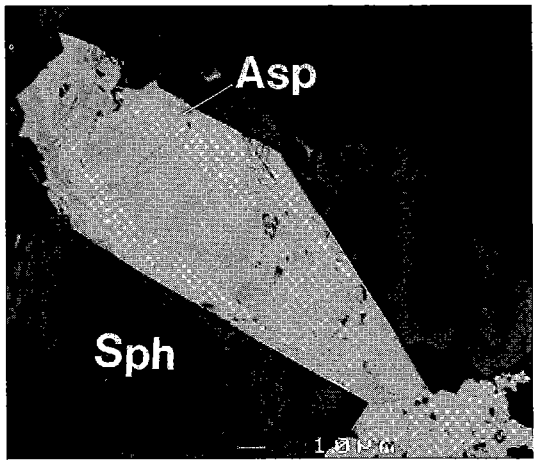

FIG. 5. Back-scattered electron image of arsenopyrite from gahnite-rich ore. Euhedral arsenopyrite (Asp) with associated subhedral to euhedral sphalerite (Sph). Arsenopyrite displays complex core-to-rim zoning, from dark, to light, with dark margins. Boundaries between zones are sharp and subparallel to grain margins. Arsenopyrite at the lower right of the image is an aggregate of fine grains, which display compositional zoning. Sphalerite also shows compositional zoning, with an Fe-poor core and Fe-rich rim. Image taken at a beam current of 3.05 nA, and an accelerating voltage of 25 kV.

component in sulfides has been documented by Wagner *et al.* (1986) and Cathelineau *et al.* (1989) using ^{197}Au Mössbauer spectroscopy, and by Zhang *et al.* (1987) using electron-spin resonance spectroscopy. Structurally bound Au can be present in arsenopyrite in amounts up to 1.5 to 1.7 wt%, although concentrations generally do not exceed 1,000 to 2,000 ppm (Johan *et al.* 1989, Cabri 1992). In many Au deposits in which arsenopyrite occurs with other Fe sulfides, arsenopyrite is the principal host for invisible Au. Pyrite can contain several hundred ppm Au (Cabri 1992), whereas pyrrhotite, chalcopyrite, and galena are relatively minor hosts for Au.

Pyrite and arsenopyrite samples from the Campbell mine were viewed with SEM at magnifications up to 43,000 times, and native Au inclusions were not observed. Gold values in pyrite grains 10 and 11 (Table 4) are high compared to other samples in this suite, but within the range of invisible Au contents reported elsewhere (Cabri 1992). Gold in pyrite and arsenopyrite from the Campbell mine is therefore present as either "colloidal" Au inclusions of less than 100 nm size, or as a structural constituent in the sulfide.

Residence of gold

The valency and residence of invisible Au in sulfides remain in question. The residence of invisible Au may involve a substitution mechanism (Johan *et al.* 1989, Wu & Delbove 1989), or presence as extremely fine "colloidal" inclusions (Cook & Chryssoulis 1990). Pyrite and arsenopyrite contain metals in octahedral coordination with six paired anions (dianions) of Y_2 and XY, respectively (Wood & Strens 1979). In pyrite, the dianion is $(S_2)^{2-}$, and XY in arsenopyrite is $(AsS)^{3-}$. This requires that Fe, which occupies the M site, be in the 2+ state in pyrite, and in the 3+ state in arsenopyrite, relations that are in accord with results from studies of magnetic susceptibility (Wood & Strens 1979) and crystal structure (Buerger 1936). Boyle (1979) first suggested that Au may be incorporated into arsenopyrite by substituting for As, on the basis of similarity of their ionic radii; a similar mechanism of substitution was suggested by Johan *et al.* (1989). However, imaging and analysis of sulfides for Au have shown correlations between As-rich growth bands in pyrite and arsenopyrite, and elevated concentrations of invisible Au (Cathelineau *et al.* 1989, Cabri *et al.* 1989, Arehart *et al.* 1993, Fleet *et al.* 1993). Furthermore, Cathelineau *et al.* (1989) and Marcoux *et al.* (1989) showed that elevated Au in arsenopyrite is associated with low levels of Sb, S, and Fe. This suggests that Au may replace Fe in arsenopyrite, and is associated with increased As in both pyrite and arsenopyrite.

Exchange of Au for As in arsenopyrite was suggested by Johan *et al.* (1989). They showed that excess As calculated in the Fe site ([M]) was inversely correlated with (Au + Sb), and proposed that the substitution $2As[M] = (Au,Sb) + Fe$ applied to the incorporation of Au in arsenopyrite. However, as noted above, most data in the literature show an increase in As with increasing Au in auriferous arsenopyrite, and a decrease in Fe with increasing Au. These relations suggest that Au replaces Fe^{3+} in the M site in arsenopyrite. To maintain charge balance, it is likely that Au is present in the 3+ state. Wu & Delbove (1989) recognized a near 1:1 correlation between Fe_{atomic} and Au_{atomic} in arsenopyrite, with a –0.79 correlation coefficient. This was interpreted to indicate the substitution mechanism Fe = Au. Recent work by Fleet & Mumin (1997) does not show this 1:1 correlation, but shows significant vacancies in the Fe site. They proposed that the arsenopyrite formula be expressed as $(Fe,As,\square)(As,Sb)_{1\pm x}S_{1\pm x}$.

Studies of auriferous pyrite have shown a relatively constant atomic proportion of As + S at ~66%, and a sympathetic increase in Au and As with a decrease in S (Fleet *et al.* 1989, Arehart *et al.* 1993). The results suggest that As in pyrite forms dianions with S as $(AsS)^{3-}$, as implied by Arehart *et al.* (1993), and that Au^{3+} replaces Fe^{2+}. Incorporation of As into pyrite may cause a structural distortion, favoring an introduction of Au (Griffin *et al.* 1991). In addition, As may form $(AsS)^{3-}$, which would favor Au^{3+} in the M site, to

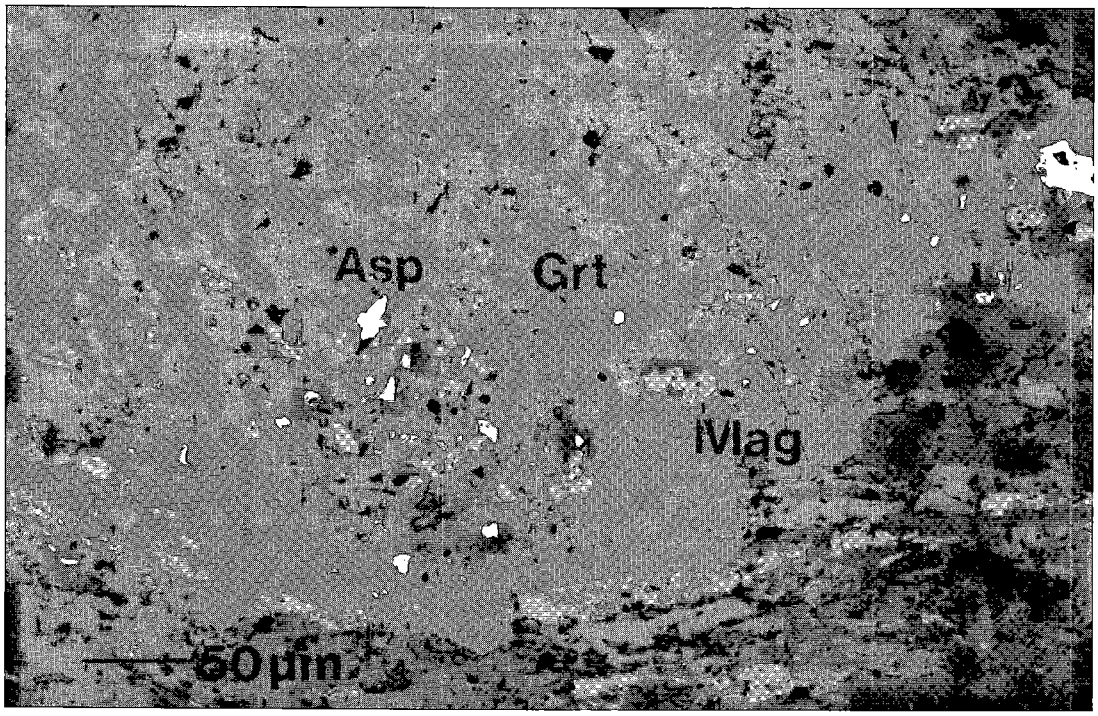

FIG. 6. Reflected-light photomicrograph of arsenopyrite within garnet. Arsenopyrite (Asp) and magnetite (Mag) included within almandine garnet (Grt). Note the helicoidal trails of inclusions (dark grey) within garnet. Sample from drill core 27–264, beneath 27th Level.

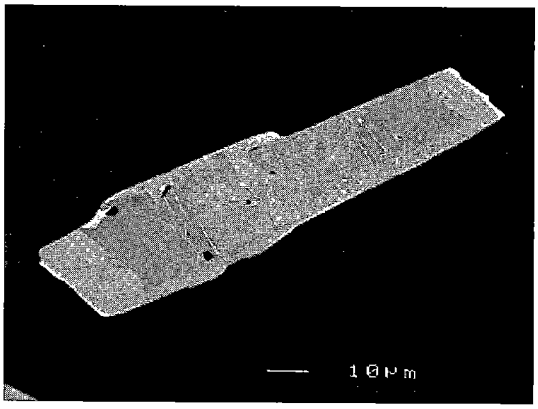

FIG. 7. Back-scattered electron image of arsenopyrite grain in garnet. Arsenopyrite with bright rim and dark core, and showing sharp boundary between rim and core. Arsenopyrite occurs as an inclusion within syntectonic almandine, and is aligned along foliation trails. Sample collected from wallrocks of the P zone.

maintain charge balance (Wood & Strens 1979, Cook & Chryssoulis 1990).

The $(As + S)_{atomic}$ in arsenopyrite from the Campbell mine is relatively constant at ~66 atom % (Table 5), and the $(As/S)_{atomic}$ ratio shows an increase in Au-rich rims. Incorporation of Au in arsenopyrite is accompanied by increasing As and decreasing S. The constant sum of As and S further implies that As replaces S, and that As may be incorporated to form the dianion $(As_2)^{4-}$. Both $(As/Fe)_{atomic}$ and $(As + Fe)_{atomic}$ increase in Au-rich rims, indicating that relative depletion in Fe occurs with Au enrichment. The data support the interpretation that Au substitutes for Fe, rather than As.

Variations in As and S, together with Au content, would be highly unlikely if Au occurs simply as very fine inclusions. Therefore, Au is likely bound as a structural component in arsenopyrite. Although Au-rich arsenopyrite rims are As-rich relative to cores, rims do not contain excess As (As/S >1). Based on similar zoning between auriferous arsenopyrite and arsenopyrite enclosed in garnet and gahnite, and the fact that all arsenopyrite examined by SIMS in this study contains elevated concentrations of Au, we conclude that arsenopyrite inclusions also are auriferous.

Timing of Hydrothermal Activity, Auriferous Mineralization and Metamorphism

Gahnite occurs in quartz–arsenopyrite ore from the eastern portions of the deposit. Gahnite is most commonly associated with metamorphosed massive sulfide deposits and their wallrocks, and may form through the desulfidation of sphalerite during prograde amphibolite-facies metamorphism (Spry & Scott 1986). Gahnite-rich spinel also occurs in granitic pegmatite, and in aluminous metasedimentary rocks in the amphibolite facies (Dietvorst 1980). The formation of gahnite-rich spinel is favored in quartz-rich assemblages, or at relatively low temperatures within the stability field of spinel (Montel *et al.* 1986).

Gahnite grains from the Campbell mine contains inclusions of sphalerite, and also is overgrown by sphalerite. Contacts between sphalerite–pyrite and gahnite are smooth to weakly dentate, suggesting that sulfide formation was in equilibrium with gahnite. In addition, textural relations between gahnite and arsenopyrite (Fig. 4) indicate that arsenopyrite deposition spanned the period of gahnite formation and was synchronous with peak metamorphism.

Zoned arsenopyrite occurs as inclusions within almandine garnet (Fig. 6), indicating that arsenopyrite growth was pre- to syn-peak metamorphism.

This study indicates that auriferous arsenopyrite is ubiquitous in the Campbell mine. Gold zoning is present in pyrite and arsenopyrite samples from both upper-greenschist-facies and lower-amphibolite-facies domains. Zoning is more complex in arsenopyrite from the veins compared to arsenopyrite from the wallrocks. Complex zoning reflects variations in hydrothermal conditions, in fluid composition, or in both. The occurrence of sharp, anhedral boundaries between Au-rich rims and Au-poor cores indicates arsenopyrite resorption and growth. Irregular growth-zoning in synthetic arsenopyrite has been recognized by Wu & Delbove (1989), and has been interpreted to result from fluctuations in $a(As)/a(S)$. In BSE images, arsenopyrite grains from the wallrock occasionally display a fractured core, filled by arsenopyrite similar to that in the rim (Fig. 7). Veins and wallrocks were intensely deformed during vein emplacement, and episodic fracture and growth of arsenopyrite are anticipated.

Arsenic is transported as H_3AsO_3 in solutions that contain H_2S as the predominant sulfur species (Heinrich & Eadington 1986). The pH boundary between the fields in which H_2S and HS^- are predominant increases with increasing temperature, with HS^- favored under increasingly alkaline conditions at higher temperatures. An extrapolation of the dissociation constant of H_2S (Ellis & Giggenbach 1971) yields $\log K = -8.89$ at 450°C, indicating that HS^- is only significant under very alkaline conditions. Alteration assemblages in greenschist-facies domains at the Campbell mine contain chlorite, carbonate, and muscovite, and lack potassium feldspar, suggesting that fluid pH was near neutral to slightly alkaline. The predominant sulfur-bearing species in the auriferous hydrothermal fluid most likely was H_2S; As was probably transported as H_3AsO_3. Deposition of arsenopyrite is facilitated by the breakdown of H_3AsO_3 during decreasing $f(O_2)$, or decreasing temperature (Heinrich & Eadington 1986). Arsenopyrite deposition may also result from increasing $a(As)$, or through an increase in $a(S_2)$. Changes in $a(S_2)$, $f(O_2)$ and temperature likely occurred during circulation of an auriferous hydrothermal fluid, as a result of fluctuations in pressure. Phase separation due to a pressure decrease would result in short-term cooling of the fluid (Drummond & Ohmoto 1985), and increases in $f(O_2)$ and $a(S_2)$ (Bowers 1991). Griffin *et al.* (1991) have interpreted As zoning in pyrite as a consequence of brecciation of the host rocks and phase separation of the hydrothermal fluid. Periodic overpressuring and phase separation are supported by the common occurrence of brecciation in ore veins at the Campbell mine and the predominance of $CO_2 + CH_4$ inclusions in ore veins (Tarnocai & Hattori 1996). This finding would account for the compositional zoning observed in the sulfides.

The application of arsenopyrite thermometry to metamorphosed sulfide deposits provides temperature estimates that generally agree with those of peak conditions of metamorphism (Sundblad *et al.* 1984, Lynch & Mengel 1995). Furthermore, arsenopyrite from metamorphosed deposits displays uniform compositions within individual grains (Sharp *et al.* 1985, Lynch & Mengel 1995). The evidence suggests that arsenopyrite easily re-equilibrates during peak metamorphism. In addition, metamorphic recrystallization of "invisible"-Au-bearing sulfides has been shown to expel Au from the pyrite (Larocque *et al.* 1995b) and arsenopyrite (Mumin *et al.* 1994) structures. Therefore, preservation of zoning in auriferous sulfides from the Campbell mine is interpreted to reflect deposition during, or after, the peak of metamorphism, as compositional zonation is unlikely to survive metamorphic recrystallization. Together with the textural relations of arsenopyrite with garnet and gahnite, the zoning in arsenopyrite suggests that auriferous hydrothermal activity was broadly synchronous with peak upper-greenschist-facies to lower-amphibolite-facies metamorphism.

Conclusions

1) Arsenopyrite and pyrite at the Campbell mine contain significant concentrations of "invisible" Au.

2) Arsenopyrite and pyrite display compositional zoning in Au, As, and S contents. Zoning indicates a peak to post-peak metamorphism introduction of Au, as zoning is not anticipated to survive upper-greenschist-facies to lower-amphibolite-facies metamorphic recrystallization.

3) The data suggest that pyrite and arsenopyrite incorporate "invisible" Au under upper-greenschist-facies to lower-amphibolite-facies metamorphic-hydrothermal conditions.

4) Occurrence of arsenopyrite in almandine garnet and auriferous arsenopyrite as inclusions within gahnite and as rosettes mantling gahnite indicate pre- to syn-peak metamorphism introduction of Au.

5) These data support a broadly syn-peak metamorphism introduction of Au at the Campbell mine.

Acknowledgements

CAT gratefully thanks the staff at the Campbell mine, especially Tom Stubens (chief mine geologist), for generous support and assistance during three summers of field work. Skillful operation of the SEM by Peter Jones (Carleton University) and SIMS by Dr. Greg McMahon (CANMET) made this study possible. We thank Gilles Laflamme and Michel Beaulne of CANMET for assistance in preparing samples for SIMS. We also thank Associate Editor J.F. Slack and two referees, M.E. Fleet and A.C. Larocque, for helpful comments on an earlier version of this manuscript. The project was funded by grants to KH from Placer Dome Canada Limited and the Natural Sciences and Engineering Research Council of Canada.

References

Andrews, A.J., Hugon, H., Durocher, M., Corfu, F. & Lavigne, M.J. (1986): The anatomy of a gold-bearing greenstone belt: Red Lake, northwestern Ontario, Canada. *In* Proc. Gold '86 Symp. (A.J. Macdonald, ed.). Konsult International, Toronto, Ontario (3-22).

Arehart, G.B., Chryssoulis, S.L. & Kesler, S.E. (1993): Gold and arsenic in iron sulfides from sediment-hosted disseminated gold deposits: implications for depositional processes. *Econ. Geol.* **88**, 171-185.

Bloem, E.J.M., Dalstra, H.J., Groves, D.I. & Ridley, J.R. (1994): Metamorphic and structural setting of Archean amphibolite-hosted gold deposits near Southern Cross, Southern Cross Province, Yilgarn Block, Western Australia. *Ore Geol. Rev.* **9**, 183-208.

Bowers, T.S. (1991): The deposition of gold and other metals: pressure-induced fluid immiscibility and associated stable isotope signatures. *Geochim. Cosmochim. Acta* **55**, 2417-2434.

Boyle, R.W. (1979): The geochemistry of gold and its deposits (together with a chapter on geochemical prospecting for the element). *Geol. Surv. Can., Bull.* **280**.

Buerger, M.J. (1936): The symmetry and crystal structure of minerals of the arsenopyrite group. *Z. Kristallogr.* **95**, 83-113.

Cabri, L.J. (1992): The distribution of trace precious metals in minerals and mineral products. *Mineral. Mag.* **56**, 289-308.

_____, Chryssoulis, S.L., De Villiers, J.P.R., Laflamme J.H.G. & Buseck, P.R. (1989): The nature of "invisible" gold in arsenopyrite. *Can. Mineral.* **27**, 353-362.

_____ & McMahon, G. (1995): SIMS analysis of sulfide minerals for Pt and Au: methodology and relative sensitivity factors (RSF). *Can. Mineral.* **33**, 349-359.

Cathelineau, M., Boiron, M.C., Holliger, P. & Denis, M. (1989): Gold-rich arsenopyrites: crystal chemistry, gold location and state, physical and chemical conditions of crystallization. *In* The Geology of Gold Deposits: the Perspective in 1988 (R.R. Keays, W.R.H. Ramsay & D.I. Groves, eds.). *Econ. Geol., Monogr.* **6**, 328-341.

Chryssoulis, S.L., Cabri, L.J. & Lennard, W. (1989): Calibration of the ion microprobe for quantitative trace precious metal analysis of ore minerals. *Econ. Geol.* **84**, 1684-1689.

Cook, N.J. & Chryssoulis, S.L. (1990): Concentrations of "invisible gold" in the common sulfides. *Can. Mineral.* **28**, 1-16.

Dietvorst, E.J.L. (1980): Biotite breakdown and the formation of gahnite in metapelitic rocks from Kemiö, southwest Finland. *Contrib. Mineral. Petrol.* **198**, 327-337.

Drummond, S.E. & Ohmoto, H. (1985): Chemical evolution and mineral deposition in boiling hydrothermal systems. *Econ. Geol.* **80**, 126-147.

Ellis, A.J. & Giggenbach, W.F. (1971): Hydrogen sulfide ionization and sulfur hydrolysis in high temperature solutions. *Geochim. Cosmochim. Acta* **35**, 247-260.

Fleet, M.E., Chryssoulis, S.L., MacLean, P.J., Davidson, R. & Weisener, C.G. (1993): Arsenian pyrite from gold deposits: Au and As distribution investigated by SIMS and EMP, and color staining and surface oxidation by XPS and LIMS. *Can. Mineral.* **31**, 1-17.

_____, MacLean, P.J. & Barbier, J. (1989): Oscillatory-zoned As-bearing pyrite from strata-bound and strataform gold deposits: an indicator of ore fluid evolution. *In* The Geology of Gold Deposits: the Perspective in 1988 (R.R. Keays, W.R.H. Ramsay & D.I. Groves, eds.). *Econ. Geol., Monogr.* **6**, 356-362.

_____ & Mumin, H. (1997): Gold-bearing arsenian pyrite and marcasite and arsenopyrite from Carlin Trend gold deposits and laboratory synthesis. *Am. Mineral.* **82**, 182-193.

Griffin, W.L., Ashley, P.M, Ryan, C.G., Sie, S.H. & Suter, G.F. (1991): Pyrite geochemistry in the North Arm epithermal Ag–Au deposit, Queensland, Australia: a proton-microprobe study. *Can. Mineral.* **29**, 185-198.

Hall, R.S. & Rigg, D.M. (1986): Geology of the west anticline zone, Musselwhite prospect, Opapimiskan Lake, Ontario, Canada. *In* Proc. Gold '86 Symp. (A.J. Macdonald, ed.). Konsult International, Toronto, Ontario (124-136).

Heinrich, C.A. & Eadington, P.J. (1986): Thermodynamic predictions of the hydrothermal chemistry of arsenic, and their significance for the paragenetic sequence of some cassiterite – arsenopyrite – base metal sulfide deposits. *Econ. Geol.* **81**, 511-527.

Johan, Z., Marcoux, E. & Bonnemaison, M. (1989): Arséno-pyrite aurifère: mode de substitution de Au dans la structure de FeAsS. *C.R. Acad. Sci. Paris* **308**, *Série* **II**, 185-191.

LAROCQUE, A.C.L., HODGSON, C.J., CABRI, L.J. & JACKMAN, J.A. (1995b): Ion-microprobe analysis of pyrite, chalcopyrite and pyrrhotite from the Mobrun VMS deposit in northwestern Quebec: evidence for metamorphic remobilization of gold. *Can. Mineral.* **33**, 373-388.

_____, JACKMAN, J.A., CABRI, L.J. & HODGSON, C.J. (1995a): Calibration of the ion microprobe for the determination of silver in pyrite and chalcopyrite from the Mobrun VMS deposit, Rouyn–Noranda, Quebec. *Can. Mineral.* **33**, 361-372.

LYNCH, G. & MENGEL, F. (1995): Metamorphism of arsenopyrite–pyrite–sphalerite–pyrrhotite lenses, western Cape Breton Island, Nova Scotia. *Can. Mineral.* **33**, 105-114.

MARCOUX, E., BONNEMAISON, M., BRAUX, C. & JOHAN, Z. (1989): Distribution de Au, Sb, As et Fe dans l'arsénopyrite aurifère du Châtelet et de Villeranges. *C.R. Acad. Sci. Paris* **308**, *Série* **II**, 293-300.

MARMONT, S. (1986): The geological setting of the Detour Lake gold mine, Ontario, Canada. *In* Proc. Gold '86 Symp. (A.J. Macdonald, ed.). Konsult International, Toronto, Ontario (81-96).

MCDONALD, D.W., DUKE, N.A. & HAUSER, R.L. (1993): Geological setting of the NERCO Con mine and the relationship of gold mineralization to metamorphism, Yellowknife, N.W.T. *Explor. Mining Geol.* **2**, 139-154.

MONTEL, J.M., WEBER, C. & PICHAVANT, M. (1986): Biotite – sillimanite – spinel assemblages in high-grade metamorphic rocks: occurrences, chemographic analysis and thermobarometric interest. *Bull. Minéral.* **109**, 555-573.

MUMIN, A.H., FLEET, M.E. & CHRYSSOULIS, S.L. (1994): Gold mineralization in As-rich mesothermal gold ores of the Bogosu–Prestea mining district in the Ashanti Gold Belt, Ghana: remobilization of "invisible" gold. *Mineral. Deposita* **29**, 445-460.

NEUMAYR, P., CABRI, L.J., GROVES, D.I., MIKUCKI, E.J. & JACKMAN, J.A. (1993): The mineralogical distribution of gold and relative timing of gold mineralization in two Archean settings of high metamorphic grade in Australia. *Can. Mineral.* **31**, 711-725.

PHILLIPS, G.N. & DE NOOY, D. (1988): High-grade metamorphic processes which influence Archaean gold deposits, with particular reference to Big Bell, Australia. *J. Metamorphic Geol.* **6**, 95-114.

ROBERT, F. & BROWN, A.C. (1981): Archean gold -bearing quartz veins at the Sigma mine, Abitibi greenstone, Quebec. II. Vein paragenesis and hydrothermal alteration. *Econ. Geol.* **81**, 593-616.

SHARP, Z.D., ESSENE, E.J. & KELLY, W.C. (1985): A re-examination of the arsenopyrite geothermometer: pressure considerations and applications to natural assemblages. *Can. Mineral.* **23**, 517-534.

SPRY, P.G. & SCOTT, S.D. (1986): The stability of zincian spinels in sulfide systems and their potential as exploration guides for metamorphosed massive sulfide deposits. *Econ. Geol.* **81**, 1446-1463.

SUNDBLAD, K., ZACHRISSON, E., SMEDS, S.-A., BERGLUND, S. & ALINDER, C. (1984): Sphalerite geobarometry and arsenopyrite geothermometry applied to metamorphosed sulfide ores in the Swedish Caledonides. *Econ. Geol.* **79**, 1660-1668.

TARNOCAI, C.A. & HATTORI, K. (1994): Extended hydrothermal activity at the Campbell gold mine, eastern Red Lake greenstone belt, Uchi Subprovince. *Geol. Assoc. Can. – Mineral. Assoc. Can., Program Abstr.* **19**, A110.

_____ & _____ (1996): Gold mineralization during peak metamorphism of greenschist - amphibolite grade at the Campbell mine, Red Lake greenstone belt, Superior Province of Canada. *Int. Geol. Congress, 30th (Beijing), Abstr.* **2**, 765.

WAGNER, F.E, MARION, P. & REGNARD, J.-R. (1986): Mössbauer study of the chemical state of gold in goldores. *In* Gold 100. Proc. Int. Conf. on Gold: Extractive Metallurgy of Gold. *S. Afr. Inst. Mining Metall.* **2**, 435-443.

WONG, L., DAVIS, D.W., KROGH, T.E. & ROBERT, F. (1991): U–Pb zircon and rutile chronology of Archean greenstone formation and gold mineralization in the Val d'Or region, Quebec. *Earth Planet. Sci. Lett.* **104**, 325-336.

WOOD, B.J. & STRENS, R.G.J. (1979): Diffuse reflectance spectra and optical properties of some sulfides and related minerals. *Mineral. Mag.* **43**, 509-518.

WU, XIN & DELBOVE, F. (1989): Hydrothermal synthesis of gold-bearing arsenopyrite. *Econ. Geol.* **84**, 2029-2032.

ZHANG, GUOWEI, HATTORI, K. & CRUDEN, A.R. (1997): Structural evolution of auriferous deformation zones at the Campbell mine, Red Lake greenstone belt, Superior Province of Canada. *Precamb. Res.* (in press).

ZHANG, Z., SIXUE, Y. & WIEN, Y. (1987): Studies of submicro-gold and lattice gold in some minerals. *J.Cent. South Inst. Mining Metall.* **15**, 355-361.

Received January 10, 1997, revised manuscript accepted June 30, 1997.